A Semi-automatic Segmentation for Tooth on Cone Beam CT Volume Following the Anatomic Guidance

Zheng Zou[1], San-ding Luo[1], Jeng-Shyang Pan[2,3] Shi-jian Liu[2,3], Sheng-hui Liao[1]

[1]School of Information Science and Engineering
Central South University
No.932, Lushannan Road, Changsha, Hunan, 410005, China
sdluo@csu.edu.cn, zouzheng84@sina.com, lsh@csu.edu.cn

[2]School of Information Science and Engineering
[3]The Key Laboratory of Big Data Mining and Applications of Fujian Province
Fujian University of Technology
No.3, Xueyuan Road, University Town, Minhou, Fuzhou, Fujian, 350118, China
jspan@cc.kuas.edu.tw, liusj2003@fjut.edu.cn

ABSTRACT. *Cone beam computed tomography(CBCT) technique is popular in three dimension imaging of the jaw bones and teeth due to its high resolution and relatively lower radiation exposure compared with multi-slice computed tomography(MSCT). But segmentation of the tooth from CBCT is challenging due to reasons such as the lower bone signal-to-noise and the topology variances. In order to accurately segment the teeth, we propose a novel volume-based interactive segmentation framework. First, valley-emphasized image is generated from original images to enhance voxels in high relief to assist the separation of tooth region from the alveolar bone with the similar intensity. Meanwhile the information about root canal is abstracted to guide the segmentation. In order to obtain the root canal curve, an energy minimization combined with the directional characterise is introduced in our method. Incorporated with the constraint offered by the root canal curve, a edge-aware harmonic field is designed to avoid leakage and shrinkage problems in the segmentation process. The experimental results demonstrated that our method is better than two other most cited methods in accuracy and efficiency.*

Keywords: Cone beam computed tomography, Root canal, Tooth segmentation, Energy minimization, Harmonic field

1. **Introduction.** Due to a high resolution and low radiation exposure, Cone Beam Computed Tomography (CBCT) is the most popular 3D imaging technique for diagnosis the jaw bones and teeth nowadays. From the dental CBCT images, segmenting and manipulation of individual tooth can offer the complete patient-specific tooth model for dental restorations, dental implant and simulation of tooth movement in dental orthodontics, which are essential steps for dental surgical navigation and showing the final orthodontic treatment effects for patients. Extracting the correct tooth boundary and accurately segmenting the individual tooth from CBCT images is challenging and difficult, mainly because of several reasons as follows. Firstly, the space between two neighboring teeth is usually very small even disappears in images due to closely arranged teeth as described in Fig. 1(a), therefore the partial boundaries of tooth may be ambiguous or invisible to be exactly defined. Secondly, the surrounding issues such as alveolar bone has similar bone density with the targeted tooth, and result in disturbance for finding the complete and
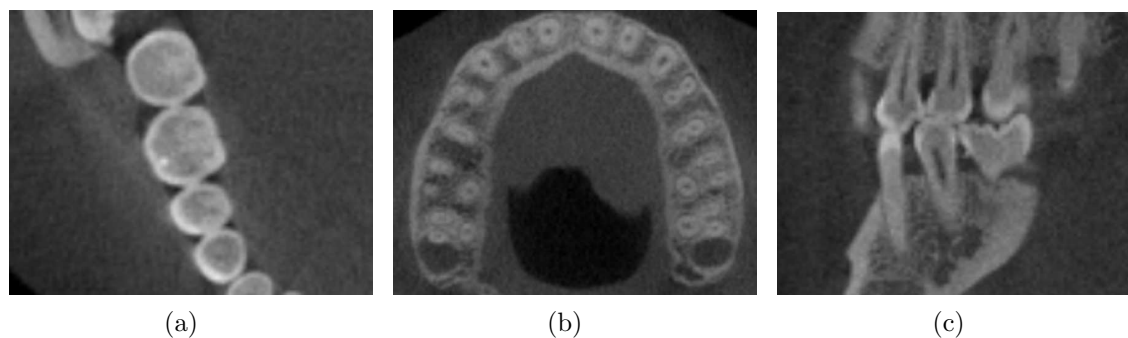
(a)   (b)   (c)

FIGURE 1. The axial view and coronal view of the jaw. (a) The adjacent tooth in axial view ; (b) Insufficient resolution and weak tooth boundaries; (c) The shape variance of the tooth in coronal view.

clear boundary as described in Fig. 1(b). Thirdly, there exists topology variance of the tooth shown in Fig. 1(c), and the number of dental root for a tooth is uncertainty. Finally, compared with common CT, CBCT images are of lower resolution and higher noise. The dental images usually contains the whole head of patient, and the mouth region to be processed is relatively smaller part relative to the head region. The actual resolution of the mouth part tends to be much less than the resolution of the whole image. In clinical, tooth segmentation is often manually operated by trained dentists, but fully partition of all teeth depending on the operation of dentist is trivial and time consuming. While the automatic or semi-automatic tooth segmentation can largely reduce workload of dentists and improve the efficiency of extracting individual tooth.

Many image segmentation methods have been proposed to solve the problem of extracting the tooth. Some conventional methods use adaptive thresholding [1] for segmenting. Due to the non-uniform intensity in the tooth region and the surrounding similar intensity tissue, thresholding may result in over segmentation or under segmentation. Chen et al. [2] propose a tooth extraction method with active contour model (ACM), which uses the local region information to iteratively evolve contour, however the contour evolvement is usually slow. Moreover, these methods based on active contour use different intensity distributions of region of interest (ROI) and background to separate each other, and fail in areas with the similar intensity levels. Therefore methods only use intensity information are not suitable for tooth segmentation on CBCT. In order to overcome the limitations of the methods above, recently some hybrid segmentation methods incorporate shape information into energy functional for optimization. Momeni and Zoroofi [3] use a multistage approach based on level set, and find the vertcial line of panoramic projection to separate individual tooth. But if teeth are not vertically aligned, this method can not accurately segment them. Gao and Chae [4] propose a adaptive active contour tracking algorithm to track the root and solve the root branching problem. The shape and intensity are used as the prior and they separate the tooth by finding a plane between two adjacent teeth along the jaw arch. The crown and the root are separately segmented with different enhanced level set based algorithms. However this method requires addition time for drawing an initial contour around each tooth before initiation. Gan et al. [15] use tooth contour propagation strategy to initialize the level set function automatically. Dong et al. [5] incorporate the tooth dentine wall into the constraint to make the contour evolution more robust. According to the priori information such as the size and the intensity for individual tooth by the training, Nguyen et al. [7] divide the teeth region into several isolated region by analyzing intensity profiles sampled in direction of the surface normal
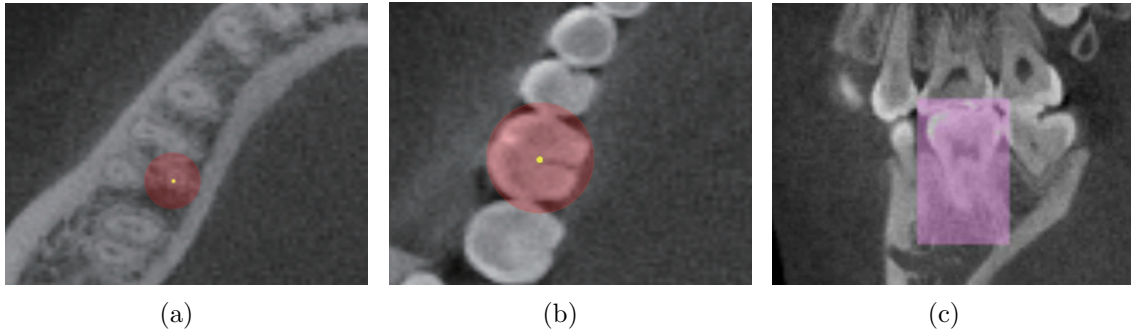
<div align="center">(a)   (b)   (c)</div>

FIGURE 2. The determination of VOI by user interaction. (a) A circular region selected by user on one slice in the top of a tooth; (b)A circular region selected by user on one slice in the bottom of a tooth ; (c) The VOI of a tooth in the coronal view.

before segmentation of tooth region, however the size priori is not robust and low resolution images usually can not offer enough profiles information for accurate segmentation, and their processing speed tends to be slow compared to the seed region growing method [14]. For most methods above, the better accuracy of performance depends on the interaction more or less. Though the interaction can offer the high level priori knowledge for the segmentation, too much interaction is time-costing and may reduce the robustness of method due to the designed interactive way.

In this paper, we propose an interactive segmentation method for accurately extracting the individual tooth on CBCT images. In order to make full use of the volumetric information for accurate segmentation, this paper segment the tooth in a volume-based way instead of the slice by slice way commonly used in existing methods. Besides the intensity and size information of the tooth, the root canal skeleton characterise abstracted from internal tooth is also used as the priori information to guide the segmentation in this paper. Without multi-parameter initialization, Harmonic field theory is used for finding the boundary of the individual tooth efficiently.

2. **Preprocessing.** To roughly extract teeth from the jaw bone, the user's input is required to acquire volume of interest(VOI) from the CBCT scan. Firstly, the user is required to specify several circular regions covering the cross-section of the tooth in slices from the top and the bottom of the tooth. Secondly, the VOI is determined by the smallest cuboid encompassing all the circles as described in Fig. 2(c).

The intensity of a tooth usually is similar as that of the alveolar bone especially in the root part of a tooth, therefore it is difficult to distinguish that neighboring region only using the gradient. In contrast, the valley [6] is more suitable in separating two adjacent objects, because it appears in the middle of two adjacent objects while gradients appear at the boundaries of each object [16]. A valley-emphasized image I_{VE} can be obtained by the morphological operations, and it is constructed by subtracting valley images I_V from an original image as defined in Eq.1, where I is an intensity value of the original image, W is the structure element, $\oplus$ denotes the dilation operation, $\ominus$ denotes the erosion operation. The valley-emphasized image is shown in Fig. 3(c), most of the voxels in the adjacent region between the tooth and the lveolar bone are improved.

$$I_{VE} = I_V - I = (I \oplus W) \ominus W) - I \qquad (1)$$

Besides, with regards to the lower resolution problem, resampling and interpolation along

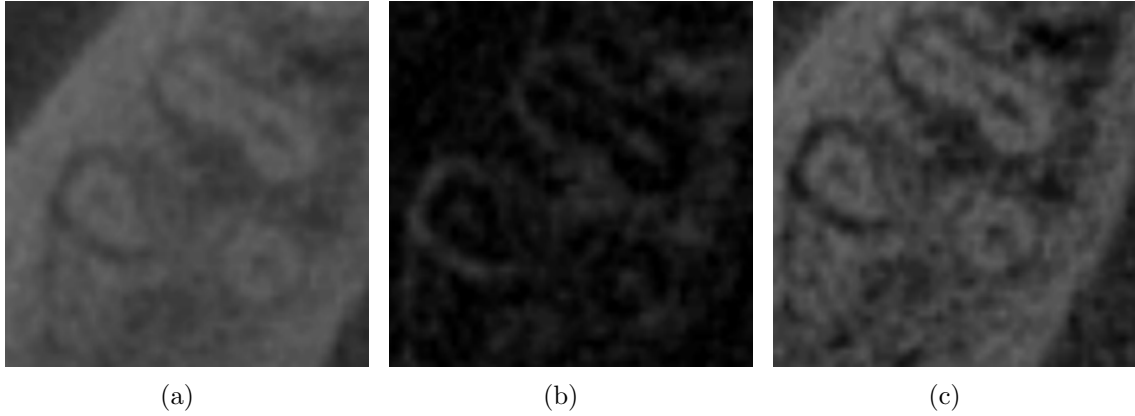(a)   (b)   (c)

FIGURE 3. The construction of the valley-emphasized image. (a) The original image ; (b) The valley images ; (c) The valley-emphasized image.

the three axial directions are used in this paper to increase the resolution, which benefits the extraction of the root canal curve in the next step.

3. **The Extraction of the root canal curve.** The root canal is a deep groove generated by radiolucent longitudinal line within the root parallel to the periodontal ligament seen on the CT scan. As a component of the integrated tooth, the various root canal configurations can reflect the trend of the internal root which is seldom used in the existing methods as a anatomic guidance. The root canal has the following properties, (a) the voxels of the root cannal region are relatively darker than others among the internal tooth region, (b) teeth may have several apical foramina, and (c) the cross sections of the root canals is irregular. As a curve in the tooth, the problem of detecting the root canal line can be converted to a new problem of finding a path between two given points, and the path should be infimum on the volume through root canal. Namely, in this section we develop the global minimal path for the groove region of the tooth.

3.1. **Constructing the energy function.** For a curve $C(s)$, s denotes the arc-length of the curve and it meets $\|\frac{\partial C}{\partial s}(s)\|^2 = 1$. All the possible path space C connects a starting point and a end point, and the designation of the energy can be described by Eq. 2

$$E(C) = \int_\Omega \omega + P(C(s))ds \tag{2}$$

where ω is a scalar constant weighting factors, and P denotes the potential function associated with local characterises of the voxels. Ω is the definition domain of the curve $C(s)$. The problem is treated as energy minimization in $A_{x_0,x}$ in Eq.3, which starts from point $C(0) = x_0$ to point $C(L) = x$.

3.2. **Definition of the root canal.** A minimal action surface U described by Eq. 3

$$U(x) = \lim_{A_{x_0,x}} \{E(C)\} = \lim_{A_{x_0,x}} \{\int_\Omega \omega + P(C(s))ds\} \tag{3}$$

denotes the minimal path of energy between x_0 and x, and each point has the energy U. The minimal action map can be related to propagating fronts emanating out of an infinitesimal circle, $\zeta(0)$ around x described in Eq. 4,

$$\|\frac{\partial \zeta(t)}{\partial t}\| = \frac{N}{P} \tag{4}$$

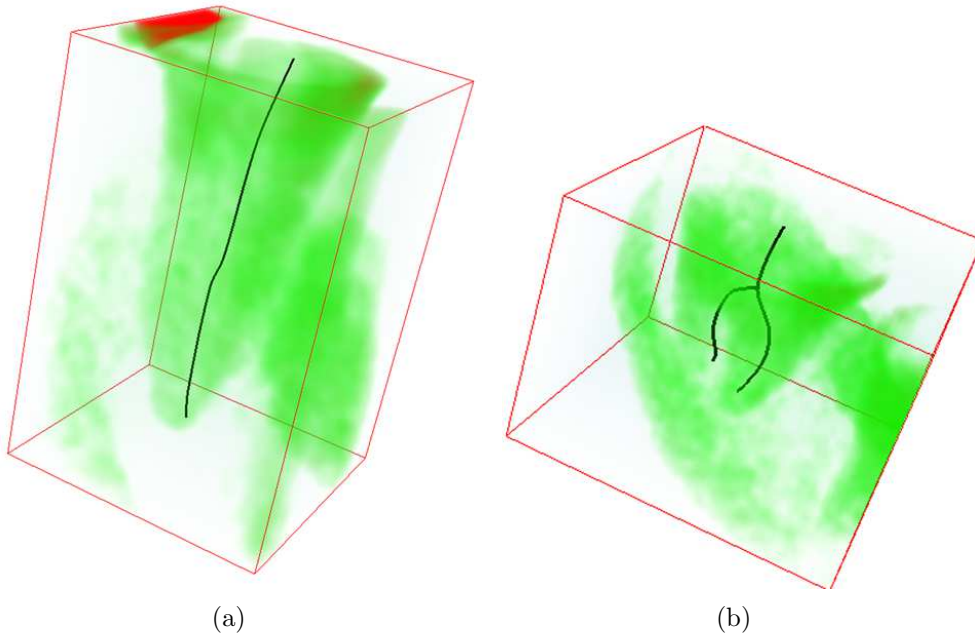(a)   (b)

FIGURE 4. The centerline result for two teeth. (a) A tooth with one apical
; (b) A tooth with two apicals .

and evolving the front over the entire image will give the value of U at every point x. $U(x)$ is the time t when the front $\zeta(0)$ passes over the point x, and U subjects to Eikonal equation in Eq. 5. As an efficient and classic method, the fast march technique [12, 13] is used in our paper for searching solution of Eikonal equation.

$$\nabla U = P \tag{5}$$

Considering that the intensity of the root canal region is lower than surrounding region, and the curve locates in the center of root canal region, we design the potential function in Eq. 6,

$$P(x) = \alpha_1 \widetilde{I}(x) + \alpha_2 L(x) + \alpha_3 T(x) \tag{6}$$

where $\widetilde{I}(x)$ denotes the intensity at location x. $max(I)$ in Eq. 7 is the maximum intensity in the volume, and α_1, α_2 and α_3 are positive constants. The intensity term implies that the potential will increase as the curve pass over the point with lower values which is normalized by $max(I)$.

$$\widetilde{I}(x) = (\frac{max(I) - I(x)}{max(I)}) \tag{7}$$

The Euclidian length of the path from the seed point is calculated with the Eikonal equation to make the path from any point to another point will have high order of continuity. $T(x)$ denotes the tangential direction at the point x, and λ_i, e_i $(i = 1, 2, 3)$ are eigenvalue and eigenvector of the structure tensor x subjected to $\lambda_1 \geq \lambda_2 \geq \lambda_3$ respectively, ν is the vector at x. The directional term in the energy guarantees that the direction of any point over the minimal path is consistent with the extension direction of the tubular root canal due. Fig. 4 demonstrates two examples for tooth, and they are of one apical and two apicals respectively. The obtained centerline result are shown with volume rendering.

$$T(x) = 1 - \sqrt{(\frac{\lambda_3}{\lambda_1}(\nu \bullet e_1))^2 + ((\frac{\lambda_3}{\lambda_2}(\nu \bullet e_2))^2 + (\nu \bullet e_3)^2} \tag{8}$$

4. **Harmonic segmentation strategy.** The harmonic field based method is a robust and recently popular way of segmenting meaningful part from the rests [10, 11]. Based on the obtained internal tooth information, to effectively find a smooth and convincing contour reflecting features faithfully, the harmonic field theory is adopted in this paper. The harmonic segmentation field φ with regard to a set of voxels should first meet the conditions that $\Delta\varphi = 0$ where Δ is the Laplacian operator, then subject to the Dirichlet boundary conditions.

4.1. **Construction of the laplacian matrix.** Constructing the harmonic segmentation field is required to firstly construct a Laplacian matrix reflecting the relationship between two neighboring voxels and the constrain for Laplacian equation. The element L_{ij} of the Laplacian matrix can be described as Eq. 9. In VOI, whether the voxel i and the voxel$j$ are neigbors depends on the 26-connected structure of the volume in our design.

$$L_{ij} = \begin{cases} \Sigma_k W_{ik}, & if \ i = j \ , \ k \neq i \\ -W_{ij}, & if \ i \ and \ j \ are \ neighbors \\ 0, & otherwise \end{cases} \qquad (9)$$

4.2. **Designation of segmentation field.** The first one is designing W_{ij} in Eq. 10, where p_i is the intensity value of voxel i, and the $Length_{ij}$ denotes the Euclidean distance between the voxel i and j, ε is a small constant to prevent zero division. The γ_{ij} is a gradient factor to enhance the weight of the edge ij with higher gradient and make the generated harmonic field more densely distributes on the region with larger gradient. The second one is the setting of constraints when solving the equation $L\varphi = 0$ by the least-squares method. In our case the voxels close to the root canal curve are set as minimuem (i.e. 0), and voxels located in the boundaries of VOI can be preset to maximum (i.e. 1).

$$W_{ij} = \gamma_{ij} \times exp(-\frac{|p_i - p_j|^2}{Length_{ij}^2 + \varepsilon}) \qquad (10)$$

4.3. **Final segmentation boundary selection.** The corresponding segmentation field are obtained by solving the linear system determined by Laplacian matrix and the constrains. The iso-surfaces of the fields is considered as the potential boundary. Denote the collection of candidate boundaries from the fields as $B = b_1, b_2, ..., b_M$, and M is the total amount of the candidate boundaries. We assign a score to each candidate for representing its confidence as a segmentation boundary. A candidate boundary with a larger gradient magnitude in segmentation field means it is likely to lie in the edge region, meanwhile the more accurate boundary is not likely of big variance in surface such as sharply raised or depressed areas. For that purpose, we introduce a gradient constraint and a shape constraint for the score to improve the robustness of selection. Specifically, we define a score S_i for each candidate as Eq. 11, and $\bar{G}_i$ denotes the average gradient magnitude along the candidate boundary. A highest score means a highest confidence that the candidate is a desirable final segmentation boundary, and the candidate with better smoothness and higher gradient can obtain higher score. To obtain the shape constraint $Shape_i$, we find the nearest neighbors $Neighbor(i)$ at the voxel i, and calculate the average angle variance between the normal of vector n_i and that of its neighbors. The neighbors of the voxel i in this paper is voxels with two-step length starting from the voxel i. The shape constraint $Shape_i$ is obtained by the average variance along the candidate boundary as described in Eq. 11, where α and β are constant factor, $N(b_i)$ and $N(Neighbor(i))$ denote the total amount of voxels over the candidate b_i and neighbour field $Neighbor(i)$ respectively. The process of generating the boundary for one tooth is shown in Fig. 5. According to the coronal, the sagittal and the transverse plane selected from the same tooth, the images are

(a)

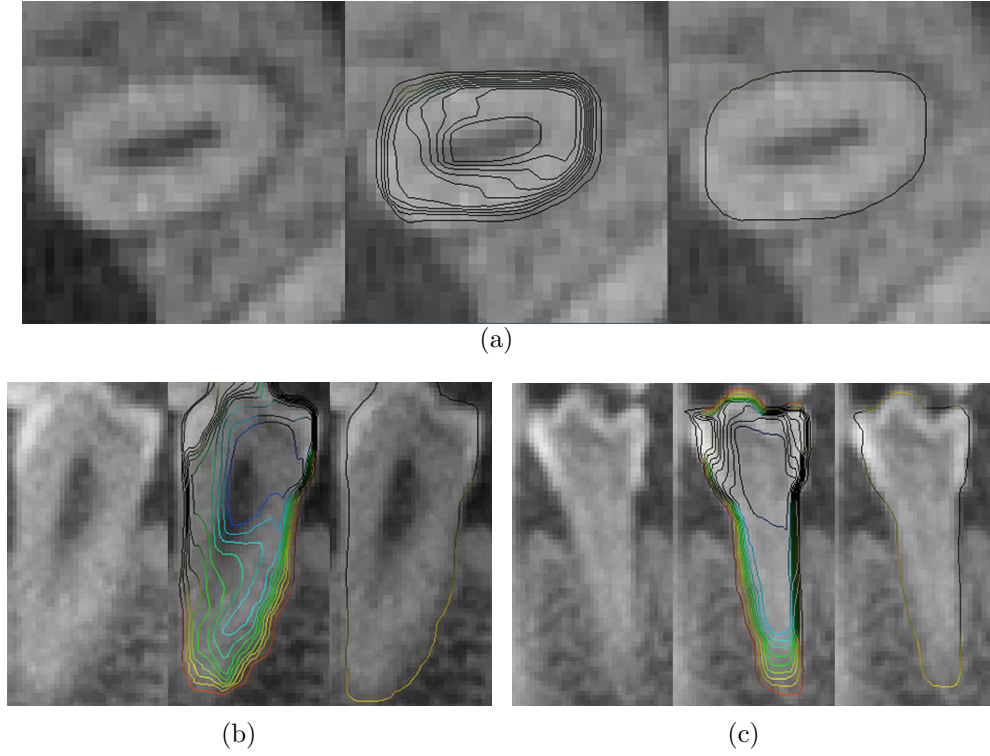(b)   (c)

FIGURE 5. The process of generating segmentation boundary for one tooth in three planes. (a) The left, the center and the right column denotes the original image , the image of segmentation field result and the image of the final boundary respectively in the transverse plane; (b) The left, the center and the right column denotes the original image, the image of segmentation field result and the image of the final boundary respectively in the sagittal plane; (c) The left, the center and the right column denotes the original image, the image of segmentation field result and the image of the final boundary respectively in the coronal plane.

divided into three groups to demonstrate the process of harmonic segmentation boundary in three planes respectively. The left column of every group is the original image, and the center column of every group is a series of candidate boundaries sampled from obtained segmentation field. All the candidates is ranked with the score, the boundary with highest score denoting the final boundary is described in the right column.

$$S_i = \alpha \bar{G}_i + \beta Shape_i = \alpha \frac{\sum_{j \in b_i} | G_j |}{N(b_i)} + \beta \frac{\sum_{j \in b_i} \frac{\sum_{k \in Neighbor(i)} (n_j * n_k)}{N(Neighbor(i))}}{N(b_i)} \qquad (11)$$

5. **Experiment results and discusses.** All evaluations were performed on an Intel Core i5 processor 3.2 GHZ with 8G RAM. Our method was implemented by C++ and the Visualization Toolkit [8] running on Windows 10. The proposed method has tested CBCT scans of eight people, which were collected at the Xiangya Hospital of Central South University from patients needing medical treatment such as the root canal therapy. In the scan, the physical spacing of neighboring voxels resolution is $0.25 \times 0.25 \times 0.25$ mm.

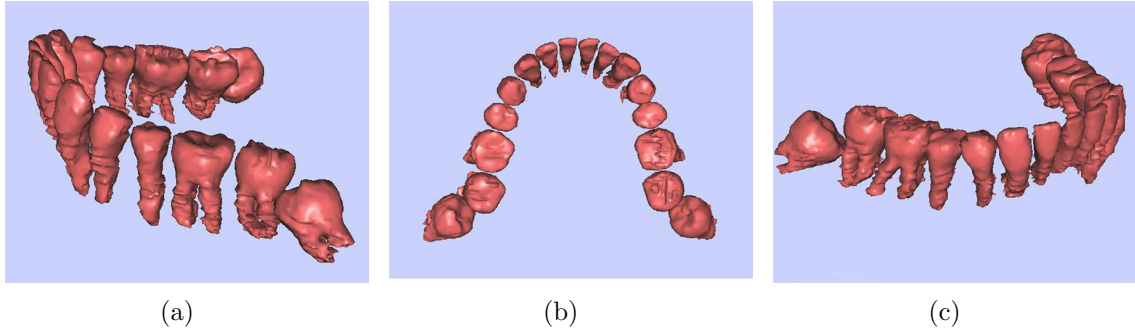(a)   (b)   (c)

FIGURE 6. The 3D mesh models of 16 teeth from our segmentation results in three different perspective. (a) The first perspective view of the segmented teeth ; (b)The Second perspective view of the segmented teeth ; (c) The Third perspective view of the segmented teeth.

5.1. **Segmentation results.** In this experiment, we used a CBCT scan with 16 individual teeth in mandible. The segmented teeth from the mandible bone are intuitively shown in Fig. 6. In order to display the final segmentation result in detail, the results is shown according to three different views. The results indicates that our method can be used to extract the individual tooth effectively even if the tooth arrange closely. To evaluate our segmentation results in accuracy, the Ground Truth (GT) results were manually segment by two experienced dentists with an image editing software on a slice-by-slice basis. For the accuracy evaluation, we use four metrics, and they are E_{fp}, E_{fn}, E_{ratio} and E_{sim} as described in Eq. 12, where V denotes tooth volxels determined by segmentation method, $Vref$ denotes tooth volxels in GT results, E_{fp} is the ratio of tooth voxels which are wrongly segmented by segmentation method according to GT results, E_{fn} is the ratio of tooth voxels which are not detected by segmentation method, E_{dif} [9] denotes the difference ratio between segmentation results and GT results. $Table 1$ summaries the segmentation errors of our tooth segmentation for eight scans. Each value is the rate of $Mean \pm standard$ deviation of all scans. The average value of E_{dif} is 2.09% ± 0.94% for all scans, indicating that the average differences between our segmentation result and GT results are less than 3%.

$$
\begin{aligned}
E_{fp} &= \frac{V-(V\cap V_{ref})}{V_{ref}} \times 100\% \\
E_{fn} &= \frac{V_{ref}-(V\cap V_{ref})}{V_{ref}} \times 100\% \\
E_{dif} &= \{1 - 2(\frac{V\cap V_{ref}}{V+V_{ref}})\} \times 100\%
\end{aligned}
\qquad (12)
$$

TABLE 1. The evaluation results for our method in accuracy

ID of the scan	E_{fp} (%)	E_{fn} (%)	E_{dif} (%)
1	2.05 ± 1.33	1.29 ± 1.56	2.05 ± 1.16
2	1.65 ± 0.92	2.87 ± 0.93	2.17 ± 1.21
3	2.44 ± 1.26	3.12 ± 1.84	3.13 ± 0.58
4	2.59 ± 0.92	1.71 ± 0.69	2.03 ± 0.87
5	1.65 ± 0.75	1.49 ± 0.48	2.16 ± 1.27
6	1.34 ± 0.93	1.53 ± 1.04	1.26 ± 0.83
7	2.92 ± 0.65	2.37 ± 0.84	2.28 ± 1.16
8	1.82 ± 0.77	1.66 ± 0.94	1.75 ± 0.52

5.2. **Comparison with others.** We compare our method with two state-of-the-art tooth segmentation method: the region growing (RG) based algorithm [14] and a level set based (LS) based algorithm [15]. Table 2 describes the comparison result in accuracy for three segmentation methods on E_{dif}. The average value of RG method is $8.93\% \pm 3.62\%$, and that of LS method is $3.75\% \pm 1.88\%$ while our method exhibits the lowest value. The average value of E_{dif} Though the results of LS method is close to ours and has better accuracy than RG method, the average processing time of each scan for LS is 996 second and ours is 826 second, obviously the consuming time of our method is less than LS. The comparison results indicates that our method had better performance in accuracy and efficiency than the others.

TABLE 2. Accuracy comparison with the others based on E_{dif}

ID of the scan	RG	LS	Our method
1	7.06 ± 3.27	3.32 ± 1.89	2.05 ± 1.16
2	8.65 ± 3.58	3.91 ± 2.26	2.17 ± 1.21
3	10.49 ± 4.42	4.77 ± 2.05	3.13 ± 0.58
4	9.36 ± 5.01	3.28 ± 1.24	2.03 ± 0.87
5	7.99 ± 4.38	2.04 ± 1.19	2.16 ± 1.27
6	9.02 ± 2.35	1.86 ± 0.97	1.26 ± 0.83
7	11.21 ± 3.73	3.81 ± 1.62	2.28 ± 1.16
8	8.89 ± 3.26	2.63 ± 0.96	1.75 ± 0.52

6. **Conclusion.** In this paper, we proposes a novel semiautomatic segmentation method to abstract the individual teeth from the whole jaw bone on CBCT images. Our proposed method depends on the anatomic characterise besides intensity neighbor and gradient information. The valley-emphasized image is generated to enhances the valley regions which in the middle of two adjacent objects for better separation of the adjacent part in neighboring tooth. The root canal curve detected by energy minimization problem is used as the anatomical guidance for the segmentation. According to the constrain of the root canal curve and local characterise of the voxels, the harmonic field is redesigned for obtaining the accurate boundary of the individual tooth. The better performance in accuracy and efficiency of our method are demonstrated in the experiments.

There is still limitation in the current method. Firstly, the case that several branches of the root canal from the same root in a tooth may converges into one branch may occurs in a few teeth. Finally, for the images scanned in a closed bite position, crowns of the mandible and maxillary would cross each other in some slices, our method is unable to extract accurate crown contours. More future works are supposed to handle these limitations.

REFERENCES

[1] H.Heo, Segmentation of tooth in CT images for the 3D reconstruction of teeth, *Proceedings of SPIE - The International Society for Optical Engineering*, vol.5298, no.2, pp.157–160.

[2] H. Chen and A. K. Jain, Tooth contour extraction for matching dental radiographs, *International Conference on Pattern Recognition, IEEE Computer Society*, vol.3, pp.522–525, 2004.

[3] M. Momeni and R. A. Zoroofi, Automated dental recognition by wavelet descriptors in CT multi-slices data, *International Journal of Computer Assisted Radiology and Surgery*, vol.3, no.6, pp.533–542, 2008.

[4] H. Gao and O. Chae, Individual tooth segmentation from CT images using level set method with shape and intensity prior, *Pattern Recognition*, vol.43, no.7, pp.2406–2417, 2010.

[5] D. X. Ji, S. H. Ong and K. W. Foong, A level-set based approach for anterior teeth segmentation in cone beam computed tomography images, *Computers in Biology and Medicine*, vol.50, no.1, pp.116–128, 2014.

[6] Y. Kim and D. Kim, A fully automatic vertebra segmentation method using 3D deformable fences, *Computerized Medical Imaging and Graphics the Official Journal of the Computerized Medical Imaging Society*, vol.33, no.5, pp.343–352, 2009.

[7] N. T. Duy, H. Lamecker and D. Kainmueller, Automatic detection and classification of teeth in CT data.*Medical Image Computing and Computer-Assisted Intervention C MICCAI 2012 Springer Berlin Heidelberg*, pp.609–616, 2012.

[8] W. Schroeder and B. Lorenson, Visualization Toolkit: An Object-Oriented Approach to 3-D Graphics, *Prentice Hall Ptr*, 2006.

[9] A. P. Zijdenbos, B. M. Dawant and R. A. Margolin, Morphometric analysis of white matter lesions in MR images: method and validation, *IEEE Transactions on Medical Imaging*, vol.13, no.4, pp.716–724, 1994.

[10] J. Jiang , C. M. Strother, Interactive decomposition and mapping of saccular cerebral aneurysms using harmonic functions: its first application with "patient-specific" computational fluid dynamics (CFD) simulations, *IEEE Transactions on Medical Imaging*, vol.32, no.2, pp.153–164, 2013.

[11] S. H. Liao, S. J. Liu and B. J. Zou, Automatic Tooth Segmentation of Dental Mesh Based on Harmonic Fields, *Biomed Research International*,vol.3, pp.1–10, 2015.

[12] J. N. Tsitsiklis, Efficient algorithms for globally optimal trajectories, *IEEE Transactions on Automatic Control*, vol.40, no.9, pp.1528–1538, 1995.

[13] J. A. Sethian, A fast marching level set method for monotonically advancing fronts, *Proceedings of the National Academy of Sciences of the United States of America*, vol.93, no.4, pp.1591–1595, 1996.

[14] H. Akhoondali, R. A. Zoroofi and G. Shirani, Rapid Automatic Segmentation and Visualization of Teeth in CT-Scan Data, *Journal of Applied Sciences*, vol.9, no.11, pp.2031–2044, 2009.

[15] Y. Gan, Z. Xia and J. Xiong, Toward accurate tooth segmentation from computed tomography images using a hybrid level set model, *Medical Physics*, vol.42, no.1, pp.14–27,2015.

[16] Y. Kim and D. Kim, A fully automatic vertebra segmentation method using 3D deformable fences, *Computerized Medical Imaging and Graphics the Official Journal of the Computerized Medical Imaging Society*, vol.33, no.5, pp.343–352, 2009.